IOPscience iopscience.iop.org

Home Search Collections Journals About Contact us My IOPscience

Transition from brittleness to ductility in SiC

This article has been downloaded from IOPscience. Please scroll down to see the full text article.

2002 J. Phys.: Condens. Matter 14 12929

(http://iopscience.iop.org/0953-8984/14/48/335)

View the table of contents for this issue, or go to the journal homepage for more

Download details:
IP Address: 171.66.16.97
The article was downloaded on 18/05/2010 at 19:14

Please note that terms and conditions apply.

INSTITUTE OF PHYSICS PUBLISHING JOURNAL OF PHYSICS: CONDENSED MATTER

J. Phys.: Condens. Matter **14** (2002) 12929–12945 PII: S0953-8984(02)53993-X

Transition from brittleness to ductility in SiC

P Pirouz[1], **M Zhang**[1], **J-L Demenet**[2] **and H M Hobgood**[3]

[1] Department of Materials Science and Engineering, Case Western Reserve University, Cleveland, OH 44106, USA
[2] Laboratoire de Metallurgie Physique, CNRS, SP2MI, 86960 Futuroscope Cedex, France
[3] Cree, Inc., 4600 Silicon Drive, Durham, NC 27703, USA

Received 27 September 2002
Published 22 November 2002
Online at stacks.iop.org/JPhysCM/14/12929

Abstract

Following an initial elastic strain, a crystal responds to an increasing external stress by either breaking up into pieces, or else plastically changing its shape before failure. In this paper, the different behaviours of a crystal—brittle cleavage versus ductile deformation—are briefly discussed, and the transition from one regime to the other is developed in a simple intuitive manner. The two responses are related and models developed for predicting the transition temperature from a brittle to a ductile behaviour. In addition, experimental measurements of the transition temperature in a wide bandgap semiconductor, 4H-SiC, are outlined and data presented. The results appear to be consistent with a transition temperature T_c recently observed in the yield stress of the same material as measured by compression experiments. However, strain rate measurements in four-point bend tests are not strictly equivalent to those in compression experiments because of the different sample geometries used in the two cases. It is thus difficult to make a direct comparison of the measured brittleness to ductility temperatures with the yield stress transitions.

1. Introduction

This paper is concerned with the behaviour of a single crystal of a semiconductor when an external stress is applied to it. In general, a monocrystal subject to an external stress, σ_{appl}, responds in one of two ways: either it yields plastically and deforms its shape or, alternatively, it fractures into two or more pieces. Since plastic deformation occurs by shearing of blocks of the crystal over slip planes along a slip direction, it is the shear component of the applied stress τ which is responsible for yielding. On the other hand, fracture of a crystal occurs by the rupture of bonds holding the atoms together across the *cleavage plane*. In the latter case, the interatomic bonds can be ruptured by *stretching* them in a direction *normal* to the cleavage plane (mode I) or, alternatively, by *shearing* the bonds in a direction *normal* (mode II) or *parallel* (mode III) to the *crack front*; mixtures of these modes can also operate. In the present paper, only mode I fracture is considered where the bonds rupture by opening the crack and

the important component of the applied stress is the tensile stress σ_n acting normal to the crack plane.

The resolved shear stress τ_{theor} for deforming a *perfect crystal*, and the normal stress σ_{theor} for fracturing it, are of the order of one-tenth of the elastic moduli (shear modulus G for yielding or Young's modulus Y for fracture) and are much larger than the values experimentally observed. Hence, both processes are believed to involve microscopic defects in the crystal; that is to say, the processes of plastic deformation and fracture take place through lattice defects that facilitate these operations. In the case of fracture, the microscopic agents are supposedly microcracks that often originate from inhomogeneities. On the other hand, plastic deformation by shearing is known to occur by the generation and motion of dislocations on the slip plane. Both microcracks and dislocations are known to nucleate relatively easily at certain heterogeneities (e.g. scratches at the surface of the crystal) and propagate or move under reasonably low stresses.

1.1. The brittle-to-ductile transition temperature

A schematic variation of the yield stress τ_y with temperature T at a constant rate of loading, or strain rate $\dot{\varepsilon}$, is shown by the solid curve in figure 1. As seen the yielding of a crystal is a thermally activated process and τ_y rises rapidly with decreasing temperature. Moreover, the whole $\tau_y(T)$ curve shifts to the right with an increase in the strain rate (see the dashed curve). Except for temperatures close to 0 K, the $\tau_y(T)$ variation can be expressed by an exponential function as follows:

$$\tau_y = A\dot{\varepsilon}^{1/n} \exp(\Delta H_\tau / k_B T) \tag{1}$$

where A and n are constants (different for the upper τ_{uy} and lower τ_{ly} yield stresses), and ΔH_τ is an energy parameter such that $n\Delta H_\tau$ is approximately the activation energy for dislocation glide ΔH_d (see, e.g., [1, 2]). Equation (1) cannot of course be used as $T \rightarrow 0$, where it would result in $\tau_y \rightarrow \infty$, instead of $\tau_y \rightarrow \tau_P$, where τ_P is the Peierls stress—defined as the stress required to move a straight dislocation from one (Peierls) valley to a neighbouring one.

Since the bond energy does not vary much with temperature, bond rupture and consequently fracture stress σ_F is expected to have a much weaker temperature dependence than the yield stress and may even be considered to be temperature independent. A schematic form of the $\sigma_F(T)$ variation is shown in figure 1 as the dot–dashed curve, where it is assumed to be linear with a weak slope. The intersection of the $\tau_y(T)$ and $\sigma_F(T)$ curves in figure 1 occurs at a temperature denoted by T_{BDT}, usually called the *brittle-to-ductile transition* (BDT) temperature. If a crystal is loaded with an increasing applied stress, σ_{appl}, at a constant rate, say $\dot{\varepsilon}$, then at temperatures below T_{BDT}, σ_{appl} reaches σ_F before reaching τ_y and the crystal fractures, i.e., the temperature range $0 < T < T_{BDT}$ represents the 'brittle regime'. On the other hand, at temperatures above T_{BDT}, σ_{appl} reaches τ_y first and the crystal yields plastically. Hence, the temperature range $T > T_{BDT}$ is the 'ductile regime' and T_{BDT} is a temperature that defines the transition between brittleness and ductility. It should be noted that the BDT temperature is not always sharp; in fact it is more appropriate to define it as $T_{BDT} \pm \Delta T$ where ΔT represents the *sharpness* or *diffuseness* of the BDT temperature. In general, this is relatively sharp in semiconductors with $0 < \Delta T < 20\,^\circ$C, depending on the crystal quality and experimental conditions. Also note from figure 1 that T_{BDT} is a function of the strain rate and increases with increasing $\dot{\varepsilon}$, i.e., the faster the crystal is loaded, the larger the temperature regime over which it behaves in a brittle manner.

In the present work, the BDT temperature has been measured in the wide bandgap semiconductor 4H-SiC, using the four-point bend technique [3]. The experimental arrangement is

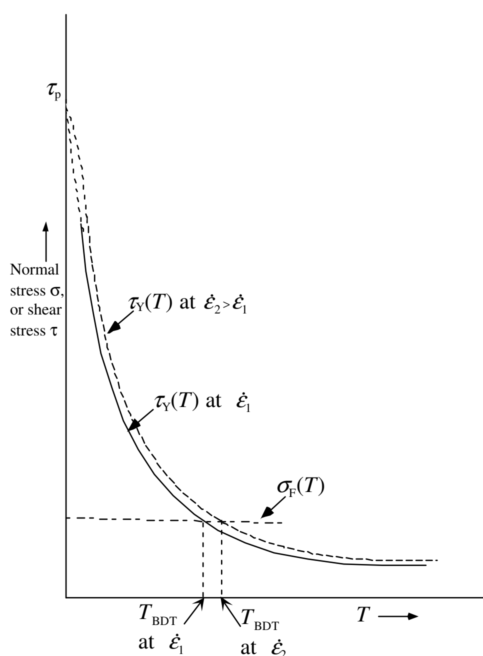

Figure 1. Schematic variations of stress versus temperature in a crystal. The solid curve shows the temperature dependence of the resolved shear stress, τ_y, needed for plastically deforming the crystal at a strain rate $\dot{\varepsilon}_1$; at a higher strain rate $\dot{\varepsilon}_2$, the curve shifts to the right (i.e., to higher temperatures) as shown by the dashed curve. Away from $T = 0$, the yield stress (solid and dashed curves) falls exponentially with increasing temperature. The variation of the fracture stress σ_F is shown schematically with a dot–dashed curve; in the figure, it is assumed this variation is linear with a very weak slope.

similar to the one used by Samuels in her BDT experiments on silicon [4]. There is, however, a significant difference in performing such measurements on silicon and other cubic semiconductors as compared to materials, like 4H-SiC, that have a hexagonal structure. In cubic semiconductors, with a face centred lattice, there are four different slip planes parallel to $\{111\}$, whereas in hexagonal semiconductors there is only one set of slip planes parallel to (0001). In both cubic and hexagonal crystals, however, there are three slip directions in each of the slip planes, parallel to $\langle 1\bar{1}0\rangle$ and $\langle 11\bar{2}0\rangle$ directions, respectively. As a result, it is much easier to activate one of the 12 $\langle 1\bar{1}0\rangle\{111\}$ slip systems in cubic semiconductors than one of the three $\langle 11\bar{2}0\rangle(0001)$ slip systems in hexagonal crystals. Also, the primary cleavage plane in cubic semiconductors is $\{111\}$ (in the case of elemental semiconductors, silicon, germanium and diamond)—or $\{1\bar{1}0\}$ (in the case of II–VI, III–V and IV–IV compounds); for hexagonal semiconductors, like ZnS, GaN or non-cubic SiC polytypes, the cleavage plane is invariably $\{10\bar{1}0\}$.

2. Experimental details

A 75 mm commercial 4H-SiC wafer (Cree, Inc.) with an off-axis tilt of 8° towards a $\langle 1\bar{2}10\rangle$ zone axis (i.e. an 8° tilt of the (0001) plane around the $\langle 10\bar{1}0\rangle$ axis relative to the surface normal) was used for the experiments.

The crystal was n-doped with a carrier concentration of $\sim 5 \times 10^{16}$ cm^{-3} (n-type). For the four-point tests, two types of sample with dimensions of $1 \times 3 \times 35$ mm^3 were cut from

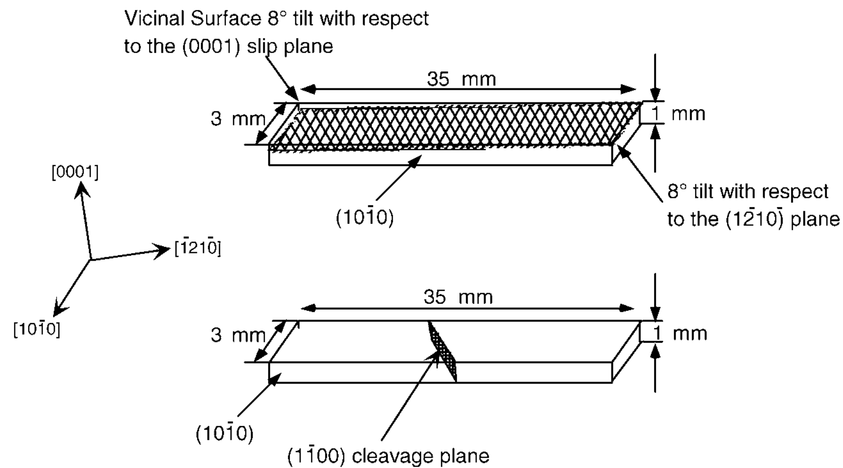

Figure 2. The orientation and dimensions of type-1 samples. Note that the cleavage plane in the lower figure makes an angle of −60° for the (1$\bar{1}$00) plane (or +60° for the (01$\bar{1}$0) plane) with respect to the front (and back) (10$\bar{1}$0) face.

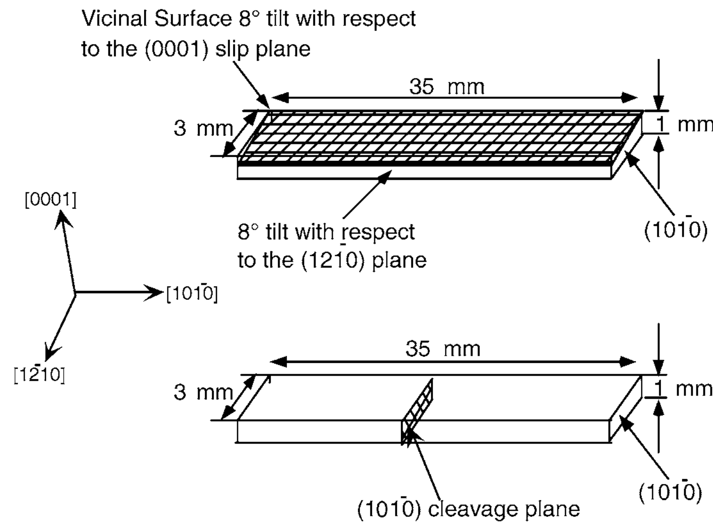

Figure 3. The orientation and dimensions of type-2 samples. Note that the cleavage plane (10$\bar{1}$0) in the lower figure is parallel to the end faces of the sample.

the wafer, as shown in figures 2 and 3. The outer and inner points of the four-point bend jig were placed, respectively, on the top and bottom 3 × 35 mm^2 faces of the sample; an Instron machine was used for loading the jig. The geometry of the four-point bend test was such that the two 1 × 3 mm^2 end faces of the sample were under a tensile stress σ_{appl} related to the applied load P by $\sigma_{appl} = 3Pd/wh^2$ where w is the sample width, h the sample height and $d = (L - l)/2$ the bending arm; l and L are, respectively, the separation of the inner and outer rollers in the four-point bend jig.

Of the two types of sample, one type was cut with the 3 mm edge (width) parallel to the [10$\bar{1}$0] axis (figure 2); such a geometry results in a finite resolved shear stress on the primary

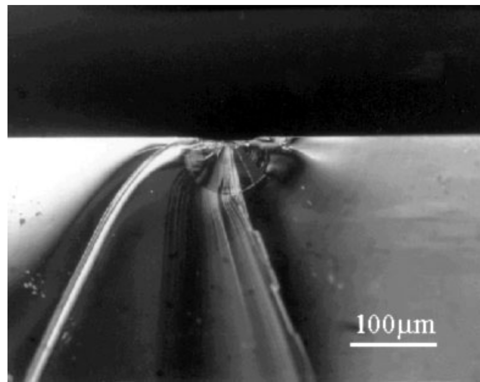

Figure 4. Semicircular radial crack of radius ∼65 μm in 4H-SiC introduced by a 1000 g Knoop indentation in a type II sample. For most experiments, the size of the radial cracks, generated by a load of 200 g, was much smaller. One of these radial cracks, with a semicircular crack front, acts as the initial microcrack for the four-point bend fracture tests.

slip system $[1\bar{2}10](0001)$ given by $\tau_{appl} = \sigma_{appl}\cos(82°)\cos(8°) = 0.138\sigma_{appl}$. Similarly, since the normal to the cleavage plane makes an angle of 30° with respect to the tensile axis (i.e., normal to the end faces of the sample in figure 2(b)), the normal stress σ_n is given by $\sigma_n = \sigma_{appl}\cos^2(30°) = 0.75\sigma_{appl}$.

In the other sample type (figure 3), the long edge (length) of the sample was along the $[10\bar{1}0]$ axis; with this geometry, there is no resolved shear stress on the (0001) slip planes. On the other hand, there is a finite normal stress σ_n on the $(10\bar{1}0)$ cleavage plane equal to σ_{appl} because the end faces of the sample are parallel to $(10\bar{1}0)$.

Precracks were introduced in both sample types by a series of five Knoop indentations, 500 μm apart, at the centre of their 3×35 mm^2 top face. In general, a Knoop indent produces a semicircular radial crack extending to the surface and terminating at the corners of its long dimension. In the example shown in figure 4, the indentation load was 1000 g and the sample was cleaved along the line connecting its far corners; the radius of the radial crack in this case is about 65 μm. In the actual tests, the Knoop indentations were made with a load of 200 g and the radial cracks had a smaller radius.

In the first sample type, the long direction of the Knoop indent was so chosen that the indentation radial crack was along a $(1\bar{1}00)$ plane; this plane makes an angle of 60° with respect to the front (and back) $(10\bar{1}0)$ faces of the sample (figure 2(b)). In the second sample type (figure 3), the long direction of the Knoop indent was parallel to the 3 mm edge of the sample and the indentation radial cracks were parallel to the $(10\bar{1}0)$ end faces (figure 3(b)). All the deformation tests were performed in high purity argon gas at temperatures between 800 and 1350 °C using four strain rates $\dot{\varepsilon} = 5.0 \times 10^{-7}$, 1.0×10^{-6}, 2.6×10^{-6} and 4×10^{-6} s^{-1}.

3. Results

Figure 5 shows the temperature dependence of stress as obtained from four-point bend tests performed on type-1 samples (figure 2) deformed at a strain rate of $\dot{\varepsilon} = 5.0 \times 10^{-7}$ s^{-1}. This figure—hereafter called a BDT plot—is typical of those obtained at all other strain rates.

The solid circles in this figure correspond to the applied stress σ_{appl} required to either fracture the sample, or to plastically deform it. The plot is divided into two parts. At each tested temperature below ∼1050 °C, the sample broke in a brittle manner whereas all the

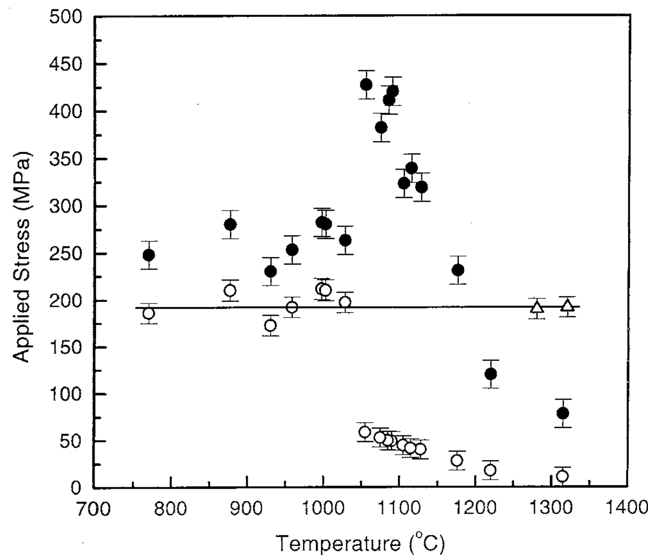

Figure 5. Temperature dependence of the applied stress σ_{appl} (solid circles) in a four-point bend test on type-1 samples of 4H-SiC at a strain rate of 5×10^{-7} s^{-1}. For temperatures below ~1050 °C, all the samples fractured at a nearly constant applied stress of 250 MPa, corresponding to a fracture stress σ_F (open circles) of ~190 MPa. For temperatures above ~1050 °C, all the samples yielded plastically; the applied stress for yielding (solid circles) decreases from ~430 MPa at 1050 °C to ~75 MPa at 1300 °C. In this ductile regime, the resolved shear stress values (i.e., yield stresses) are shown by open circles. The two open triangles correspond to tests at 1280 and 1320°C on type II samples.

samples yielded plastically at temperatures above ~1050°. Thus, 1050 ± 15 °C corresponds to the BDT temperature T_{BDT} at this strain rate. In the brittle regime ($T < T_{BDT}$), the applied stress required to break the samples was 250 ± 15 MPa at all the tested temperatures. The component of σ_{appl} normal to the cleavage plane, i.e., the normal stress σ_n, is shown by an open circle at temperatures below T_{BDT}. In the ductile regime ($T > T_{BDT}$), the solid circles in the figure correspond to the applied stress that resulted in yielding of the samples; here, the open circles show the resolved shear stress on the primary slip system i.e., yield stress, $\tau_y = \sigma_{appl} \cos 8° \cos 82°$. At any temperature in this range, the yield stress is very close to the literature value of the upper yield point as determined in bulk deformation tests of 4H-SiC by Samant [5] or by Demenet [6, 7].

Considering the solid circles in this figure, it can be seen that the applied stress is nearly constant in the brittle regime with a value $\sigma_{appl} = 250 \pm 15$ MPa, corresponding to a fracture stress of $\sigma_F = \sigma_n = \sigma_{appl} \cos^2 30° = 190 \pm 15$ MPa. At a temperature of about 1050 °C, there is a sudden rise in the stress applied to the sample. This abrupt increase of σ_{appl} comes about because, at this temperature, the crystal undergoes a BDT whereby the applied stress of ~250 MPa no longer suffices to propagate the crack front. The reason is that dislocations start emitting from the crack tip (semicircular in figure 4), thus blunting it and also acting to shield the tip from the applied tensile stress. Consequently, the material no longer fractures at a stress of σ_F because it has become ductile and a much larger stress of ~430 MPa has to be applied to generate dislocations and move them, something that results in shearing the crystal and plastically deforming it. From then on, as new samples are tested at consecutively higher temperatures, the stress required for generating an avalanche of dislocations at the crack tip and moving them away keeps decreasing. This is similar to the decrease of the upper yield point with temperature in bulk deformation tests.

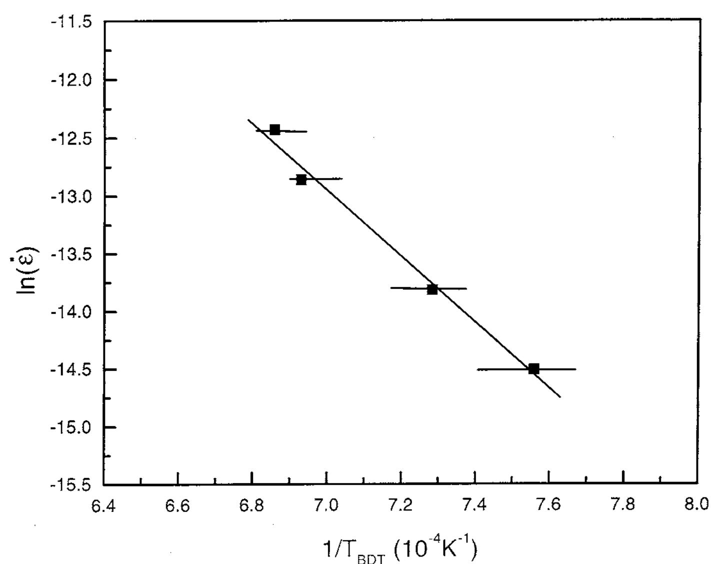

Figure 6. T_{BDT} increases logarithmically with $\dot{\varepsilon}$ and a plot of $\ln(\dot{\varepsilon})$ versus $1/T_{BDT}$ is linear. This Arrhenius plot has a slope corresponding to an activation energy of 2.47 ± 0.2 eV in 4H-SiC.

The shape of the BDT plots for type-1 samples tested at other strain rates is much the same as that shown in figure 5 except for a shift of T_{BDT} to higher temperatures with increasing strain rates. On the other hand, the shape of the plots for type-2 samples is very different. In fact, all these samples fractured in a brittle manner over the whole temperature range tested up to 1350 °C. Two representative points, for type-2 samples tested at $T = 1300$ and 1350 °C are shown by open triangles in figure 5. The reason that there is no BDT in type-2 samples is the absence of any resolved shear stress on the primary slip system $[1\bar{2}10](0001)$ and, consequently, insufficient dislocation activity (generation and/or motion) even at higher temperatures to blunt the crack tip and shield it from the applied tensile stress. Consequently, the radial precrack rapidly expands when the applied stress σ_{appl} reaches the critical value σ_F, resulting in catastrophic failure of the sample. Although only two points for type-2 samples, at $T = 1300$ and 1350 °C, are shown in figure 5, the fracture stress σ_F was in fact the same at all temperatures, equal to that in the brittle regime of type-1 samples, i.e. about 190 MPa.

As mentioned in section 2, the BDT temperature shifts to higher temperatures with increasing rates of applied loading. To see the dependence of the BDT temperature on the strain rate, T_{BDT} was determined at four different strain rates, $\dot{\varepsilon} = 5.0 \times 10^{-7}$, 1.0×10^{-6}, 2.6×10^{-6} and 4×10^{-6} s^{-1}. With increasing strain rate, the abrupt rise in the BDT plot systematically shifted to the right indicating an exponential relationship between $\dot{\varepsilon}$ and T_{BDT}. Figure 6 is a plot of $\ln(\dot{\varepsilon})$ versus $1/T_{BDT}$. As in other semiconductors, this is an Arrhenius plot which, in the present case, has a slope corresponding to an activation enthalpy of 2.47 ± 0.2 eV.

In the introduction, it was pointed out that the microscopic incidence of fracture proceeds by the propagation of pre-existing, or freshly nucleated, microcracks. At a crack tip, the local tensile stress is magnified by a factor that depends on its radius of curvature and the crack length. Consequently, the resistance of a material to fracture, i.e., its resistance to crack propagation and catastrophic failure, not only depends on the tensile stress applied to the material but also on the shape and dimensions of microcracks present in it; hence it is dependent on the thermo-mechanical history of the material. This fracture resistance property of a material is sometimes

referred to as its *fracture toughness* and often characterized by a parameter called the *critical stress intensity factor*, K_c. For a semi-elliptical surface flow in bending, the fracture toughness K_c is given by

$$K_c = \sigma_F M \left(\frac{\pi c}{Q} \right)^{1/2} \tag{2}$$

where M is a free surface correction factor, c is the crack length and Q is a so-called 'flaw shape parameter' (see, e.g., [8]).

In most of the four-point bend tests, the initial precracks were introduced by Knoop microindentation using an indentation load of 200 g. The size of the radial crack depends of course on the indentation load. To check whether the precrack size affects the BDT results, a number of four-point fracture experiments were performed with larger precrack sizes generated by higher load Knoop indentations. Substitution of these values of fracture stresses and corresponding precrack sizes in equation (2) results in a fracture toughness of 1.9 ± 0.3 MPa $m^{1/2}$ for 4H-SiC.

4. Discussion

There have been basically three approaches to the BDT in a crystal in the literature. In the first approach, BDT is considered to occur when nucleation of dislocations at the crack tip becomes energetically favourable with respect to the rupture of interatomic bonds during propagation of the crack front. This approach was first proposed in a pioneering paper by Kelly *et al* [9] and was subsequently improved upon by Rice and Thomson [10] and other investigators. The second approach, based on the mobility of dislocations, started after St John [11] reported that the BDT temperature in silicon is sensitively dependent on the strain rate, and $\ln(\dot{K})$ versus $1/T_{BDT}$ is an Arrhenius plot with a slope equal to that for dislocation glide. Perhaps the most comprehensive of the models based on dislocation mobility is the work of Hirsch and co-workers (see, e.g., [12] for the original model and, e.g., [13] for the modified one). A third approach was taken by Khanta *et al* who considered the BDT to be a Kosterlitz–Thouless type of instability (see, e.g., [14]). For some interesting recent work on the latter type of model, see the paper of Sun *et al* [15]. In the following, we shall discuss the transition from a brittle behaviour to a ductile one using two approaches. The first one develops the simple intuitive model presented in section 1.1 (figure 1). The second approach is based on recent experiments that extended the measurement of the yield stress of a few semiconductors to the brittle regime (see, e.g., [16] for a number of III–V semiconductors, and, e.g., [6, 7, 17, 18] for 6H- and 4H-SiC). In these experiments, a critical temperature T_c was observed at which there was a transition from one mode of slip to another. The closeness of T_c to T_{BDT} led to the proposal that these two temperatures are in fact identical [19–21].

4.1. First approach

The first approach simply quantifies the intuitive picture of the BDT temperature presented in figure 1. Assuming that the fracture stress σ_F is temperature independent, then the intersection of the two curves in figure 1 can be obtained by substituting $\tau_F = S\sigma_F$ for τ_y in equation (1):

$$\tau_F = S\sigma_F = A\dot{\varepsilon}^{1/n} \exp\left(\frac{\Delta H_\tau}{k_B T} \right)$$

where S is a geometrical (e.g. Schmid) factor relating the normal stress σ_n to the shear stress τ. This results in the following expression for the BDT temperature:

$$T_{BDT} = \frac{\Delta H_\tau}{k_B \ln\left(\frac{S\sigma_F}{A\dot{\varepsilon}^{1/n}}\right)}. \tag{3}$$

According to this equation, a plot of $\ln(\dot{\varepsilon})$ versus $1/T_{BDT}$ should be a straight line with a slope $-n\Delta H_\tau/k_B$ and an intercept $n\ln(S\sigma_F/A)$. Since $n\Delta H_\tau$ is approximately equal to the activation energy for dislocation glide ΔH_d, the slope of this plot should give $\Delta H_d/k_B$. This was actually first suggested by St John [11] who, in a classical series of experiments on silicon, determined the BDT temperature, sharpness of the transition and dependence of T_{BDT} on the strain rate, and showed that the $\ln(\dot{\varepsilon})$ versus $1/T_{BDT}$ plot has a slope corresponding to the activation energy for dislocation velocity in silicon. St John's important results in silicon [11] were later verified by a number of authors and the same found to be true in a few other semiconductors for which T_{BDT} has been measured as a function of the strain rate (e.g., [4, 22–26])

To test the validity of equation (3) for estimating the BDT temperature, we consider the example of silicon where there is an abundance of data on the temperature dependence of the yield stress as well as on its fracture stress. As mentioned before, equation (1) is valid for both the upper and lower yield stresses, τ_{uy} and τ_{ly}, respectively, however with different values of n and ΔH_τ. In the case of dislocation-free intrinsic silicon, Patel and Chaudhuri [27] determined $n = 2.4$, $\Delta H_\tau = 0.94$ and $n\Delta H_\tau \approx \Delta H_d \approx 2.3$ eV for the upper yield stress. Other authors have measured the temperature dependence of the yield stress for dislocated crystals and come up with slightly different values. Thus, Yonenaga and Sumino [28] determined n and ΔH_τ in a silicon crystal with an initial dislocation density N_0 of 2×10^4 cm^{-2}; the values they obtained were 2.4 and 1.25 eV for τ_{uy}, and 3.3 and 0.8 eV for τ_{ly}. In order to estimate T_{BDT} from equation (3), the constant A must be first determined. Using the aforementioned data of Yonenaga and Sumino on intrinsic silicon ($N_0 = 2 \times 10^4$ cm^{-2}) [28], the upper yield stress at $T = 800\,^\circ$C and $\dot{\varepsilon} = 10^{-5}$ s^{-1} is $\tau_{uy} \approx 10$ MPa, which, together with the τ_{uy} parameters ($n = 2.4$, $\Delta H_\tau = 1.25$ eV) in equation (1), gives $A \approx 1718$. Similarly, according to Yonenaga and Sumino [28], the lower yield stress of silicon ($N_0 = 2 \times 10^4$ cm^{-2}) at $T = 800\,^\circ$C and $\dot{\varepsilon} = 10^{-5}$ s^{-1} is $\tau_{ly} \approx 7$ MPa, which, together with the relevant τ_{ly} parameters ($n = 3.3$, 0.8 eV) in equation (1), gives $A \approx 37\,144$. There is also extensive literature on the fracture stress of silicon; thus, in intrinsic silicon, Samuels [4] measured σ_F to be ~300 MPa. In her samples, the precrack was made parallel to the (111) plane, with the tensile axis normal to this plane. In this case, the largest Schmid factor is on the $[101](11\bar{1})$ {or the $[011](11\bar{1})$ or the $[110](1\bar{1}1)$} system with $S = 2/3\sqrt{6}$. Hence, one obtains

$$T_{BDT} = \frac{\Delta H_\tau}{k_B \ln\left(\frac{S\sigma_F}{A\dot{\varepsilon}^{1/n}}\right)} = \frac{14\,506}{\ln\left(\frac{47\,526}{(\dot{\varepsilon})^{1/2.4}}\right)} \tag{4}$$

using the τ_{uy} parameters, and

$$T_{BDT} = \frac{\Delta H_\tau}{k_B \ln\left(\frac{S\sigma_F}{A\dot{\varepsilon}^{1/n}}\right)} = \frac{9284}{\ln\left(\frac{2198}{(\dot{\varepsilon})^{1/3.3}}\right)} \tag{5}$$

using the τ_{uy} parameters.

From equations (4) and (5) for T_{BDT}, table 1 is obtained, comparing Samuels' experimental results (for a precrack radius of 13 μm) [4] with the predicted values.

The τ_y results obtained for 4H-SiC by the compression tests allow us to compare T_c and T_{BDT} in this material. According to [6], at a temperature of 1030 °C and a strain rate of $\dot{\varepsilon} = 2.6 \times 10^{-6}$ s^{-1}, the yield stress is $\tau_y \approx 36$ MPa. Taking an activation energy of 4.5 eV for

Table 1. Comparison of the BDT temperature T_{BDT} of intrinsic silicon from experiments of Samuels [4] and theory (equations (4) and (5)). (Note: the experimental values are somewhere in between the values predicted by equations (4) and (5).)

$\dot{\varepsilon}$ (s^{-1})	1.3×10^{-6}	2.6×10^{-6}	5.2×10^{-6}	1.3×10^{-5}	2.6×10^{-5}
T_{BDT} (K/°C)[a]	835/562	858/585	868/595	906/633	930/657
T_{BDT} (K/°C)[b]	884/611	899/626	916/643	938/665	956/683
T_{BDT} (K/°C)[c]	787/514	801/528	815/542	836/563	852/579

[a] Experiment from [4].
[b] Predicted using the τ_{uy} parameters, equation (4).
[c] Predicted using the τ_{ly} parameters, equation (5).

Table 2. Comparison of the critical transition temperature T_c of 4H-SiC from experiments of Demenet *et al* [6, 7] and the predicted BDT temperatures from theory (equation (6)). (Note: the differences are less than 100 °C.)

$\dot{\varepsilon}$ (s^{-1})	2.6×10^{-6}	3.6×10^{-5}	3.6×10^{-4}
T_c (K/°C)[a]	1303/1030	1373/1100	1433/1160
T_{BDT} (K/°C)[b]	1207/934	1285/1012	1363/1090

[a] Experiment (from [6]).
[b] Predicted from equation (6).

Table 3. Comparison of BDT temperature T_{BDT} of 4H-SiC from experiments of Zhang *et al* [3] and theory (equation (7)). (Note: this time, the differences are larger specially at higher strain rates.)

$\dot{\varepsilon}$ (s^{-1})	5.0×10^{-7}	1.0×10^{-6}	2.6×10^{-6}	4.0×10^{-6}
T_c (K/°C)[a]	1323/1050	1373/1100	1443/1170	1458/1185
T_{BDT} (K/°C)[b]	1248/975	1269/996	1299/1026	1313/1040

[a] Experiment (from [3]).
[b] Predicted from equation (7).

dislocation glide in 4H-SiC (from [6]), and assuming a value of 3 for n, we get $\Delta H_\tau = 1.5$ eV. From this, equation (1) gives $A = 3826$ which, together with $\sigma_F = 190$ MPa (from figure 5) and $S = 0.5$, reduces equation (3) to

$$T_{BDT} = \frac{\Delta H_\tau}{k_B \ln\left(\frac{S\sigma_F}{A\dot{\varepsilon}^{1/n}}\right)} = \frac{17\,391}{\ln\left(\frac{24\,830}{\dot{\varepsilon}^{1/3}}\right)} \tag{6}$$

giving the comparisons between experimental values of T_c and theoretical values of T_{BDT} as in table 2.

We can also compare the experimental and predicted values of T_{BDT} for 4H-SiC. In this case, we need to use $S = 0.138$ for the four-point bend tests used in the fracture experiments. Equation (3) then reduces to

$$T_{BDT} = \frac{\Delta H_\tau}{k_B \ln\left(\frac{S\sigma_F}{A\dot{\varepsilon}^{1/n}}\right)} = \frac{17\,391}{\ln\left(\frac{8939}{\dot{\varepsilon}^{1/3}}\right)} \tag{7}$$

giving table 3.

4.2. *Second approach*

In the previous approach to the problem, an estimate of T_{BDT} was made by identifying this temperature with the intersection of the $\tau_y(T)$ and $\sigma_F(T)$ curves. In the second approach, we shall consider the nucleation of dislocations at the crack tip which blunt the tip and shield it

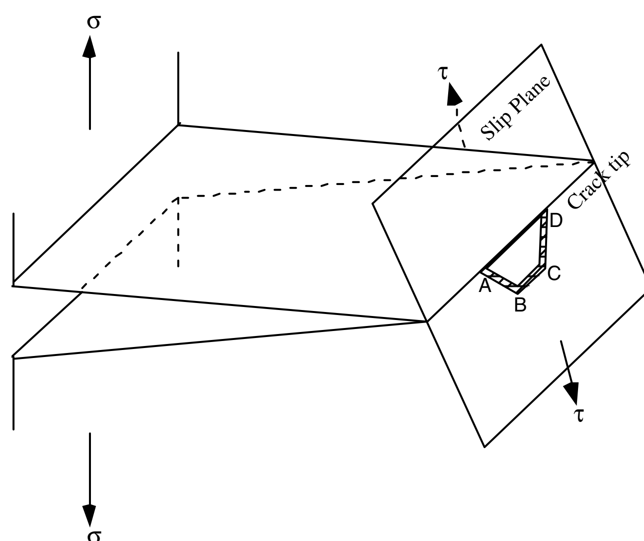

Figure 7. A crack tip under mode-I loading (crack-opening mode). The resolved shear stress on the slip plane intersecting the crack tip is τ. This has resulted in the nucleation of a (dissociated) dislocation at some crack tip heterogeneity, e.g. a ledge.

with their back-stress. This is closer to the original suggestion of Kelly *et al* [9] that was later developed into the Rice–Thomson model [10].

The presence of a crack in a solid modifies the stress (and displacement) field in the vicinity of the tip. For instance, the stress at the tip of an elliptical crack of length (major axis) $2c$ and radius of curvature ρ is magnified by a factor c^2/ρ. Consequently, when dealing with local stresses in the vicinity of a crack in a solid, it is more appropriate to use another parameter, the stress intensity factor K (or K_I when considering mode I), rather than the stress tensor σ_{ij}. In general, at a point r from the tip of a *line* crack, and inclined at an angle θ with respect to the crack plane, the relation between K_I and the components of stress tensor σ_{ij} is

$$\sigma_{ij} = \frac{K_I}{\sqrt{2\pi r}} f_{ij} \qquad (8)$$

where f_{ij} is a geometrical factor (see, e.g., [29]).

The problem can now be considered with the help of figure 7. Here a tensile stress σ is applied to a sample containing a crack of length c, resulting in a stress intensity factor K_I on the crack tip.

The question now is whether, at a certain temperature T, increasing the stress intensity factor K_I makes it first reach the critical value K_{Ic}—whereby the crack propagates catastrophically and the sample fails—or whether it increases the resolved shear stress on the most highly favoured slip system sufficiently to result in dislocation nucleation before K_I reaches K_{Ic}. If we consider a constant $\dot{K}$ fracture test, as in figure 8, the stress intensity factor K_I increases linearly with time. From this figure, the time taken to reach K_{Ic} is $(K_{Ic} - K_0)/\dot{K}$, where K_0 is the stress intensity factor before the loading cycle starts; this is the 'background' or residual stress intensity factor, say, from the presence of internal stresses (e.g., other dislocations) in the crystal.

As mentioned before, we shall assume that the crystal is ductile at a temperature T if a sufficient number of dislocations nucleate at the crack tip to blunt and shield it from the applied

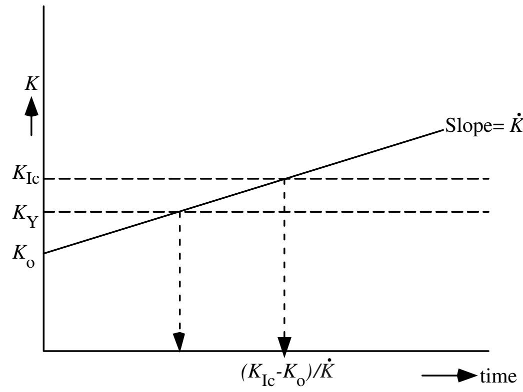

Figure 8. Variation of the stress intensity factor K_I in a constant $\dot{K}$ fracture test. When K_I reaches the critical value K_{Ic}, the crystal fractures in a catastrophic manner. On the other hand, if K_I reaches K_y before K_{Ic}, the resolved shear stress τ_y on the slip plane is large enough (reducing the effective nucleation activation enthalpy ΔH_n^{eff} sufficiently) that dislocations are generated at the crack tip (as in figure 7).

tensile stress. Otherwise, the stress intensity factor K_I keeps increasing until it reaches K_{Ic} and brittle fracture occurs. The simplest assumption would be that the crystal becomes ductile as soon as the first dislocation forms. Assuming dislocation nucleation to be thermally activated, with an activation barrier ΔH_n, then the mean time for the nucleation of a dislocation at a temperature T is $1/\nu_0 \exp\left(\frac{\Delta H_n}{k_B T}\right)$, where ν_0 is a frequency factor ($\approx 10^{13}$ s^{-1}). Thus we can assume that a crystal is ductile if a dislocation forms before K_I reaches K_{Ic}, i.e., that $1/\nu_0 \exp\left(\frac{\Delta H_n}{k_B T}\right) \leqslant (K_{Ic} - K_0)/\dot{K}$.

It is known that in the absence of stress, the activation enthalpy for dislocation nucleation is very large, of the order of 100 eV or so, implying that it would take an enormous amount of time for a dislocation to form purely by thermal activation. On the other hand, it is also known that the activation barrier is reduced in the presence of large stresses, say, at a sharp crack tip, where stress concentration takes place. Let the global applied stress τ be magnified by a factor α at the crack tip such that the crack tip stress is $\alpha\tau$. Then $\Delta H_{eff}^n = \Delta H_n - \alpha\tau V^*$ is the *effective activation enthalpy* for the nucleation of dislocations, given by lowering of the stress-free enthalpy ΔH_n by the effective stress $\alpha\tau$ at the crack tip. In this equation V^* is the activation volume. Hence one can take the criterion for ductility to be the following expression:

$$\frac{1}{\nu_0} \exp\left[\frac{(\Delta H_n - \alpha\tau V^*)}{k_B T}\right] \leqslant \frac{(K_{Ic} - K_0)}{\dot{K}}$$

or

$$\frac{1}{\nu_0} \exp\left(\frac{\Delta H_{eff}^n}{k_B T}\right) \leqslant \frac{(K_{Ic} - K_0)}{\dot{K}}.$$

Assume that dislocation nucleation takes place when the stress intensity factor K reaches K_y (before reaching K_{Ic}), where K_y is the stress intensity factor corresponding to the yield stress τ_y. Then the effective activation enthalpy is reduced to $\Delta H_n^{eff} = \Delta H_n - \alpha\tau_y V^*$, and the condition for ductility reduces to

$$\frac{1}{\nu_0} \exp\left[\frac{(\Delta H_n - \alpha\tau_y V^*)}{k_B T_{BDT}}\right] = \frac{(K_y - K_0)}{\dot{K}} \tag{9}$$

Table 4. Comparison of the 4H-SiC yield stress transition temperature T_c, as determined by compression tests [6, 7], with the BDT temperature T_{BDT}, as determined by four-point bend tests (present experiments).

$\dot{\varepsilon}$ (s^{-1})[a]	2.6×10^{-6}	3.6×10^{-5}	3.6×10^{-4}	—
T_c (°C)	1030	1100	1160	—
$\dot{\varepsilon}$ (s^{-1})[b]	5.0×10^{-7}	1.0×10^{-6}	2.6×10^{-6}	4.0×10^{-6}
T_{BDT} (°C)	1050	1100	1170	1185

[a] Compression.
[b] Four-point bend.

or

$$T_{BDT} = \frac{(\Delta H_n - \alpha \tau_y V^*)}{k_B \ln\left[\frac{\nu_0 (K_y - K_0)}{\dot{K}}\right]} = \frac{\Delta H^n_{eff}}{k_B \ln\left[\frac{\nu_0 (K_y - K_0)}{\dot{K}}\right]}. \tag{10}$$

According to this equation, a plot of $\ln(\dot{K})$ versus $1/T_{BDT}$ should be a straight line with a slope $\Delta H^n_{eff}/k_B$, proportional to the effective activation enthalpy for nucleation of *perfect* dislocations, and an intercept $\ln[\nu_0(K_y - K_0)]$.

Since the stress intensity factor K_I and the normal stress σ_n are related by a geometrical factor (say, χ), we can write $K_I = \chi \sigma_n = \chi \tau / S$, where τ is the resolved shear stress and S is the Schmid factor S. Also the rate of change of the stress intensity factor $\dot{K}$ is related to the strain rate $\dot{\varepsilon}$ by $\dot{K} = \chi \dot{\sigma} = \chi Y \dot{\varepsilon}$. Substituting for K_y, K_0 and $\dot{K}$ in equation (10), we get

$$T_{BDT} = \frac{\Delta H^n_{eff}}{k_B \ln\left[\frac{\nu_0 (\tau_y - \tau_0)}{SY\dot{\varepsilon}}\right]} = \frac{\Delta H^n_{eff}/k_B}{\ln\left[\frac{\nu_0}{SY}(\tau_y - \tau_0)\right] - \ln(\dot{\varepsilon})}. \tag{11}$$

If the crack tip is under a compressive stress, σ_0 is negative (as is K_0 in equation (10)) thus making $(K_y - K_0)$ larger and shifting T_{BDT} to lower temperatures. Conversely, if the crack tip is under a tensile stress, σ_0 is positive (as is K_0 in equation (10)) thus making $(K_y - K_0)$ smaller and shifting T_{BDT} to higher temperatures. As a first approximation, however, assume that, at the start of the loading cycle, the stress is zero and thus $\tau_0 = 0$ in equation (11) (or $K_0 = 0$ in equation (10)). In this case, the BDT temperature is given by

$$T_{BDT} = \frac{\Delta H^t_{eff}/k_B}{\ln\left(\frac{\nu_0}{Y}\sigma_y\right) - \ln(\dot{\varepsilon})}. \tag{12}$$

4.3. Transition temperature in the yield stress and modification of the second approach

It is well established that a semi-logarithmic plot of the yield stress—as determined by deformation experiments on bulk semiconductors—versus $1/T$ is a straight line with a slope proportional to the activation energy for dislocation velocity [1, 2]. This is basically what would be expected from equation (1). Recently, low temperature deformation experiments on a number of semiconductors [16], including bulk 6H- and 4H-SiC [6, 17], have shown that, at a critical temperature T_c, there is a sharp change in the slope of the $\ln[\tau_y(1/T)]$ plot, implying that different deformation mechanisms operate at temperatures above and below T_c. This critical transition temperature in the $\tau_y(T)$ behaviour appears to be close to the BDT temperature T_{BDT} of the tested semiconductor. Thus, in 4H-SiC, T_c is about 1000 °C (close to the BDT temperatures determined in this work) and, moreover, shifts with a change in the strain rate in the same manner as T_{BDT}. Table 4 compares the critical temperature T_c in 4H-SiC, as determined from compression experiments [6, 7], with the BDT temperature T_{BDT}, from the present four-point bend tests.

Recalling that the temperature dependence of the yield stress was determined by uniaxial compression tests whereas the BDT temperatures were measured by four-point bend tests, the differences in the magnitude of the transition temperatures at different strain rates can be appreciated, and the agreement between the two sets of results may be considered reasonable. Thus, a sample of, say, gauge length 10 mm, undergoing a four-point bend test in a machine operated at a crosshead displacement rate of, say, 10 μm min^{-1}, will be strained at a rate nearly three orders of magnitude slower than a sample of the same gauge length undergoing a compression test in the same machine with the same cross-head speed!

During the compression experiments on 4H-SiC, the microstructure of the deformed samples was characterized by TEM for samples deformed below and above T_c. The results were interesting in that they showed that deformation in both temperature ranges $T < T_c$ and $T > T_c$ occurs by the formation and motion of dislocations, even though the density of deformation-induced dislocations (and the corresponding strain) was far lower in samples deformed at low temperatures ($T < T_c$) than that in samples deformed at high temperatures ($T > T_c$). However, the most significant difference between the deformation-induced dislocations appearing at $T < T_c$ versus those appearing at $T > T_c$ was in their character: all the deformation-induced dislocations generated in the low temperature regime ($T < T_c$), as characterized by TEM, turned out to be single leading partials on parallel slip planes each dragging a stacking fault [5, 6, 17, 18]. This was very different from higher temperature experiments (at $T > T_c$), in the ductile regime of SiC, where all deformation-induced dislocations were found to be perfect, albeit dissociated leading/trailing partial pairs bounding a ribbon of intrinsic stacking fault. Based on these results, it was hypothesized that the BDT takes place at the temperature at which trailing partials first nucleate [19, 20]; in other words, the critical temperature T_c was identified with the BDT temperature T_{BDT}. Based on this identification, a model was presented whereby the activation enthalpies ΔH^l_{eff} and ΔH^t_{eff} for the nucleation of leading and trailing partials were assumed to be different with $\Delta H^t_{eff} > \Delta H^l_{eff}$. Moreover, it was argued that, even in the brittle regime, leading partial dislocations do nucleate and move giving rise to a limited amount of strain [21]. However, according to the model, nucleation of single leading partials is not sufficient to make the crystal ductile, because each nucleation event at the crack tip prevents nucleation of a subsequent leading partial (see figure 9), i.e. partial dislocation multiplication from any one source stops after the first leading partial is emitted.

The condition for ductility is now a matter of nucleating the trailing partial dislocations. In this case, the same expression as equation (10) is obtained except that the activation enthalpy corresponds to that of the trailing partial, ΔH^t_{eff}, rather than the perfect, dislocation, i.e.

$$T_{BDT} = \frac{(\Delta H^t_n - \alpha\tau_y V^*)}{k_B \ln\left[\frac{\nu_0(K_y - K_0)}{\dot{K}}\right]} = \frac{\Delta H^t_{eff}}{k_B \ln\left[\frac{\nu_0(K_y - K_0)}{\dot{K}}\right]}. \quad (13)$$

In this sense, the onset of BDT coincides with the nucleation of the trailing partial dislocations at the crack tip.

Formally, there is not much difference between equations (10) and (13) because the velocity (and, thus, the corresponding activation energy ΔH^n_{eff}) of a perfect (dissociated) dislocation is effectively determined by the slow partial (the one having a larger activation enthalpy, ΔH^t_{eff}), implying that $\Delta H^n_{eff} \approx \Delta H^t_{eff}$. The microscopic details of the two models, however, are very different. In the model where nucleation of perfect dislocations corresponds to the onset of ductility, there is simply no dislocation activity at any temperature below T_{BDT}. On the other hand, in the model where nucleation of the trailing partial is identified with the transition criterion, limited dislocation activity is expected even at temperatures lower than T_{BDT}. In other words, nucleation of the trailing partial is like a switch that turns on 'massive' dislocation activity (by, e.g., operation of Frank–Read sources, half-loop generation from heterogeneities etc).

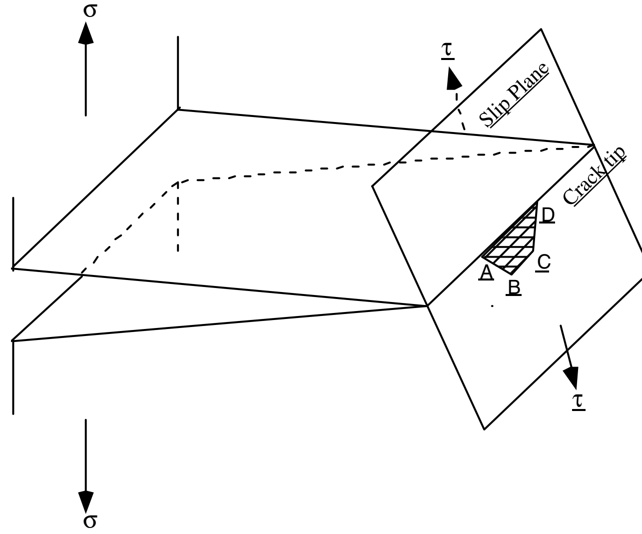

Figure 9. Nucleation of leading partial dislocations at crack tip heterogeneities (dislocation sources) is not sufficient to make the crystal ductile because, once formed, the stacking faults dragging behind the partials prevent further nucleation events from the same sources and the sources effectively shut off. Hence, in the brittle regime, only a few leading partials can be formed at the ledges or other crack heterogeneities without the formation of an avalanche of perfect dislocations that can blunt the crack tip.

We can check for the validity of equation (13) by taking a value of 2.47 eV for the effective activation enthalpy ΔH^t_{eff} (from figure 6). The predicted T_{BDT} values in this case turn out to be underestimated by a few hundred degrees. To get reasonable agreement with the experimental values, the effective activation energy for nucleation of the trailing partial turns out to be over 4 eV. It is interesting that the slope of the experimental plot of $\ln(\tau_y)$ versus $1/T$ at high temperatures [6, 7] gives a value of 4.5 ± 0.3 eV at $\dot{\varepsilon} = 2.6 \times 10^{-6}$ and 3.6×10^{-4} s^{-1}, and 5.1 ± 0.3 eV at $\dot{\varepsilon} = 3.6 \times 10^{-5}$ s^{-1} (the slope of the $\ln(\dot{\varepsilon})$ versus $1/T_{BDT}$ plot gives the very high value of ~6.1 eV). Taking $\Delta H^t_{eff} = 4.5$ eV, we get the following equation for T_{BDT}:

$$T_{BDT} = \frac{\Delta H^t_{eff}}{k_B \ln\left[\frac{\nu_0(\tau_y - \tau_0)}{SY\dot{\varepsilon}}\right]} = \frac{52\,220}{\ln\left(\frac{483\tau_y}{\dot{\varepsilon}}\right)} \tag{14}$$

from which table 5 is obtained.

These is an overestimate of more than 100 °C in the predicted values of the yield stress transition temperatures T_c. Using the same value of activation enthalpy, the experimental and predicted BDT temperatures are compared in table 6:

There is some improvement, resulting in reasonable agreement between the model and experimental T_{BDT} values. Again, the role of widely differing strain rates in the two types of test is not clear.

The discussion in this section leads us to conclude that the application of the nucleation model to the BDT event in 4H-SiC indicates an effective activation enthalpy for dislocation nucleation (of the order of 4 eV) that is substantially higher than the activation energy for dislocation glide (2.47 eV).

Table 5. Comparison of the critical temperature T_c in 4H-SiC, determined by compression tests (see [6, 7]), with the values predicted from equation (14).

$\dot{\varepsilon}$ (s^{-1})[a]	2.6×10^{-6}	3.6×10^{-5}	3.6×10^{-4}
τ_y (MPa)[b]	~36	72.6	80.2
T_c (K/°C)[c]	1303/1030	1373/1100	1433/1160
T_c (K/°C)[d]	1433/1160	1513/1240	1616/1343

[a] Compression tests [6, 7].
[b] From [6, 7].
[c] Experiment [6, 7].
[d] From equation (14).

Table 6. Comparison of the BDT temperature T_{BDT} in 4H-SiC, determined by four-point bend tests (present experiments), with the values predicted from equation (14).

$\dot{\varepsilon}$ (s^{-1})[a]	5.0×10^{-7}	1.0×10^{-6}	2.6×10^{-6}	4.0×10^{-6}
τ_y (MPa)	50	50	50	50
T_{BDT} (K/°C)[b]	1323/1050	1373/1100	1443/1170	14581185
T_{BDT} (K/°C)[c]	1359/1086	1384/1111	1420/1147	1437/1164

[a] Four-point bend tests.
[a] Experiment [3].
[b] From equation (14).

5. Conclusion

The transition from brittleness—where the crystal fails by fracture—to ductility—where the crystal deforms plastically by dislocation formation and motion—has been discussed in terms of two approaches. In one, the transition is identified with the temperature at which the stress required to yield the crystal plastically becomes less than the stress required to rupture the bonds and fracture the crystal. Quantification of this model provides an expression for the BDT temperature T_{BDT} that exhibits a linear dependence of logarithm of the strain rate with $1/T_{BDT}$. The slope of this curve is approximately proportional to the activation energy for dislocation glide, consistent with experiments of St John and others on silicon and other semiconductors. In the other approach, the BDT is identified with the temperature at which nucleation of dislocations from crack tip heterogeneities (e.g. ledges) first can occur. In this case also, the derived expression predicts an Arrhenius relationship between the logarithm of the strain rate and $1/T_{BDT}$. However, the slope is now predicted to be proportional to the activation energy for dislocation nucleation rather than dislocation glide. Finally, a series of tests to determine the BDT temperature in 4H-SiC has been presented and compared with the predictions of the two models.

Acknowledgments

PP would like to thank the National Science Foundation (grant number DMR-0108303) and the Basic Energy Sciences Division of the Department of Energy (grant number FG02-93ER45496) for supporting this work.

References

[1] Alexander H 1986 Dislocations in covalent crystals *Dislocations in Solids* vol 7, ed F R N Nabarro (Amsterdam: Elsevier) pp 114–234

[2] Rabier J and George A 1987 Dislocations and plasticity in semiconductors. II. The relation between dislocation dynamics and plastic deformation *Rev. Phys. Appl.* **22** 1327–51

[3] Zhang M, Hobgood H M, Demenet J L and Pirouz P 2002 On the brittle-to-ductile transition temperature in 4H-Si *J. Mater. Res.* submitted

[4] Samuels J 1987 The brittle to ductile transition in silicon *DPhil Thesis* University of Oxford

[5] Samant A V, Hong M H and Pirouz P 2000 The relationship between activation parameters and dislocation glide in 4H-SiC single crystals *Phys. Status Solidi* b **222** 75–93

[6] Demenet J-L, Hong M H and Pirouz P 2000 Plastic behaviour of 4H-SiC single crystals deformed at low strain rates *Scr. Mater.* **43** 865–70

[7] Demenet J-L 2001 unpublished data

[8] Anstis G R, Chantikul P, Lawn B R and Marshall D B 1981 A critical evaluation of indentation techniques for measuring fracture toughness: I. Direct crack measurements *J. Am. Ceram. Soc.* **64** 533–8

[9] Kelly A, Tyson W R and Cottrell A H 1967 Ductile and brittle crystals *Phil. Mag.* **15** 567–86

[10] Rice J R and Thomson R 1974 Ductile versus brittle behaviour of crystals *Phil. Mag.* **29** 73–97

[11] St John C 1975 The brittle-to-ductile transition in pre-cleaved silicon single crystals *Phil. Mag.* **32** 1193–212

[12] Hirsch P B, Roberts S G and Samuels J 1989 The brittle–ductile transition in silicon: II. Interpretation *Proc. R. Soc.* A **421** 25–53

[13] Hirsch P B and Roberts S G 1991 The brittle–ductile transition in silicon *Phil. Mag.* A **64** 55–80

[14] Khanta M, Pope D P and Vitek V 1994 Dislocation screening and the brittle-to-ductile transition: a Kosterlitz–Thouless type instability *Phys. Rev. Lett.* **73** 684–7

[15] Sun Y-Q, Hazzledine P M and Hirsch P B 2002 Cooperative nucleation of shear dislocation loops *Phys. Rev. Lett.* **88** 65503–6

[16] Suzuki T, Yasutomi T, Tokuoka T and Yonenaga I 1999 Plasticity of III–V compounds at low temperatures *Phys. Status Solidi* a **171** 47–52

[17] Samant A V, Zhou W L and Pirouz P 1998 Effect of temperature and strain rate on the yield stress of monocrystalline 6H-SiC *Phys. Status Solidi* a **166** 155–69

[18] Samant A V 1999 Effect of test temperature and strain-rate on the critical resolved shear stress of monocrystalline α-SiC *PhD Thesis* Case Western Reserve University

[19] Pirouz P, Samant A V, Hong M H, Moulin A and Kubin L P 1999 On temperature-dependence of deformation mechanism and the brittle–ductile transition in semiconductors *J. Mater. Res.* **14** 2783–93

[20] Pirouz P, Samant A V, Hong M H, Moulin A and Kubin L P 1999 On deformation and fracture of semiconductors *Microscopy of Semiconducting Materials (Inst. Phys. Conf. Ser. No. 164)* ed A G Cullis and R Beanland (Bristol: Institute of Physics Publishing) pp 61–6

[21] Pirouz P, Demenet J L and Hong M H 2001 On transition temperatures in plasticity and fracture of semiconductors *Phil. Mag.* A **85** 1207–27

[22] Brede M and Haasen P 1988 The brittle-to-ductile transition in doped silicon as a model substance *Acta Metall.* **36** 2003–18

[23] Samuels J and Roberts S G 1989 The brittle–ductile transition in silicon: I. Experiments *Proc. R. Soc.* A **421** 1–23

[24] Michot G and George A 1989 Fracture and crack tip plasticity in silicon and gallium arsenide *Int. Symp. on Structure and Properties of Dislocations in Semiconductors (Inst. Phys. Conf. Ser. No 104)* ed S G Roberts, D B Holt and P R Wilshaw (Bristol: Institute of Physics Publishing) pp 385–96

[25] Brede M 1993 The brittle-to-ductile transition in silicon *Acta Metall. Mater.* **41** 211–28

[26] Serbena F C and Roberts S G 1994 The brittle-to-ductile transition in germanium *Acta Metall. Mater.* **42** 2505–10

[27] Patel J R and Chaudhuri A R 1963 *J. Appl. Phys.* **34** 2788

[28] Yonenaga I and Sumino K 1978 Dislocation dynamics in the plastic deformation of silicon crystals: I. Experiments *Phys. Status Solidi* a **50** 685–93

[29] Lawn B E and Wilshaw T R 1975 *Fracture of Brittle Solids* (Cambridge: Cambridge University Press)